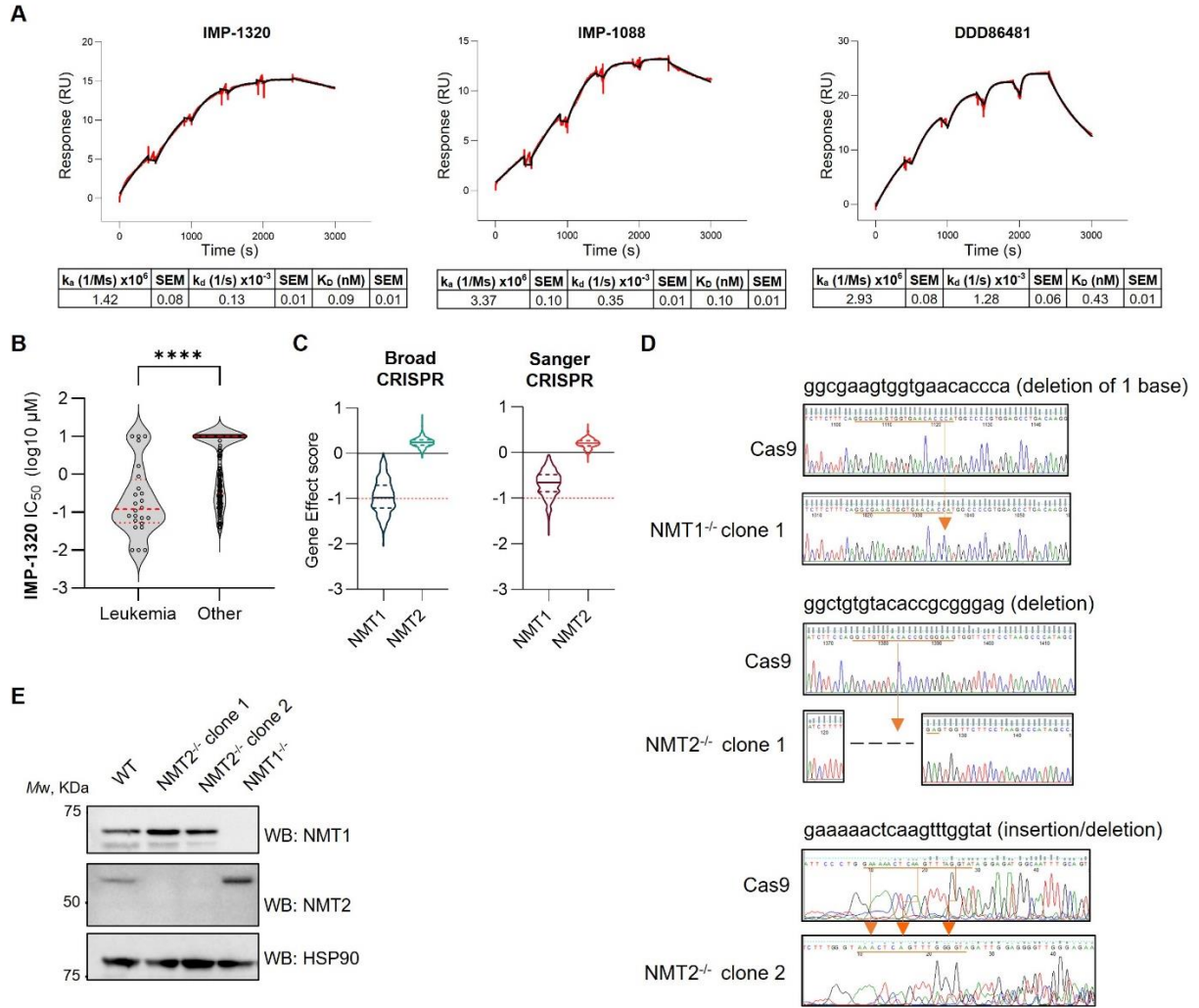


**Supplemental information**

**MYC deregulation sensitizes cancer cells  
to *N*-myristoyltransferase inhibition**

**Gregor A. Lueg, James Zhang, Monica Faronato, Andrii Gorelik, Wouter W. Kallemijn, Francesco Falciani, Josephine Walton, Jack W. Houghton, Silvia Vannini, Evon Poon, Barbara M. Costa, Roberto Solari, Robin Carr, Andrew S. Bell, Edward J. Bartlett, Bernadette Brzezicha, Martin Janz, Louis Chesler, Dinis P. Calado, and Edward W. Tate**



**Figure S1: Validation of NMTi and genetic factors influencing NMTi, related to Figure 1. (A)** Representative SPR sensorgrams of single cycle kinetics measurements of NMTi used in this study interacting with recombinant NMT1. Sensorgrams were fitted to a 1:1 model, (black lines). Kinetic constants for binding are shown below. SEM: Standard error of the mean. **(B)** The distribution of  $IC_{50}$  values in the cell line panel for leukemia lines compared to those of all other lineages (Student's t-test, two-tailed). \*\*\*\*  $P < 0.0001$  **(C)** Gene effect scores for *NMT1* and *NMT2* for sgRNA libraries, analyzed using the Broad pipeline. Red dashed line: median gene effect scores of genes classified as core essential. **(D)** Representative chromatograms of PCR products from wild type and mutant alleles, including insertions and/or deletion, in the modified HeLa cell line. The sequence of the gRNA primer is shown on top of the chromatogram and targeted regions are highlighted by arrows. **(E)** Western blot for NMT1 or NMT2 in CRISPR-Cas9 mediated knockout and wild type HeLa cells.

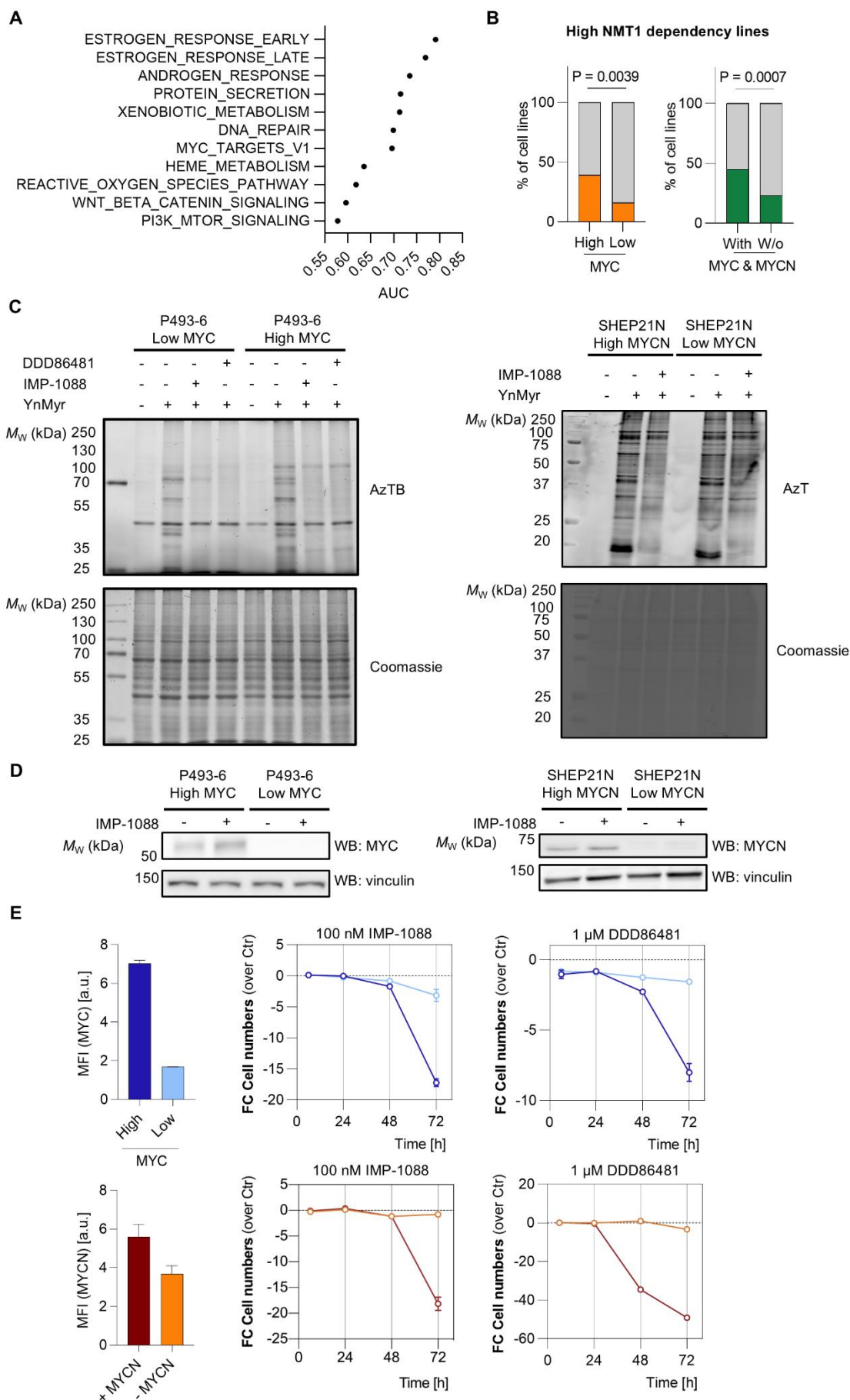


**Figure S2: MYC deregulation sensitizes cancer cells to NMTi, related to Figure 2. (A)** AUC values of the ROC curves for the significantly differentially expressed Hallmark gene sets in IMP-1320 sensitive vs less sensitive cells. **(B)** Representation of NMT1-dependent cell lines among lines expressing high MYC (by quantiles), or with structural alterations in MYC or MYCN loci (Fisher-Exact test, Sanger Project Score). **(C)** NMTi target engagement in P493-6 (left) and SHEP21N (right) cells as determined by in-gel fluorescence assays. P493-6 cells were treated with IMP-1088 (100 nM) or DDD86481 (1  $\mu$ M) and YnMyr for 18 h and lysates subjected to ligation with Azido-TAMRA-biotin (AzTB). SHEP21N cells were treated with IMP-1088 (100 nM) and YnMyr for 18 h and lysates subjected to ligation with Azido-TAMRA (AzT). **(D)** Western blot for MYC or MYCN in P493-6 (left) or SHEP21N (right) cells respectively with or without IMP-1088 (100 nM, 24 h) treatment. The image for MYCN has been contrast adjusted from the original (min-max range set to 0-15054) to improve legibility using ImageJ; see Figure S9 for the original image data. **(E)** Impact of NMTi on viable cell number in P493-6 (top) and MYCN-ER-SHEP (bottom) cell lines. Left, flow cytometry analysis and quantification of MYC or MYCN. Middle, fold-change in cell numbers upon IMP-1088 treatment (100 nM), measured over time by flow cytometry. Right, fold-change in cell numbers upon DDD86481 treatment (1  $\mu$ M), measured over time by flow cytometry. Data in **(E)** are shown as mean  $\pm$  s.e.m. of at least n = 2 biological replicates.

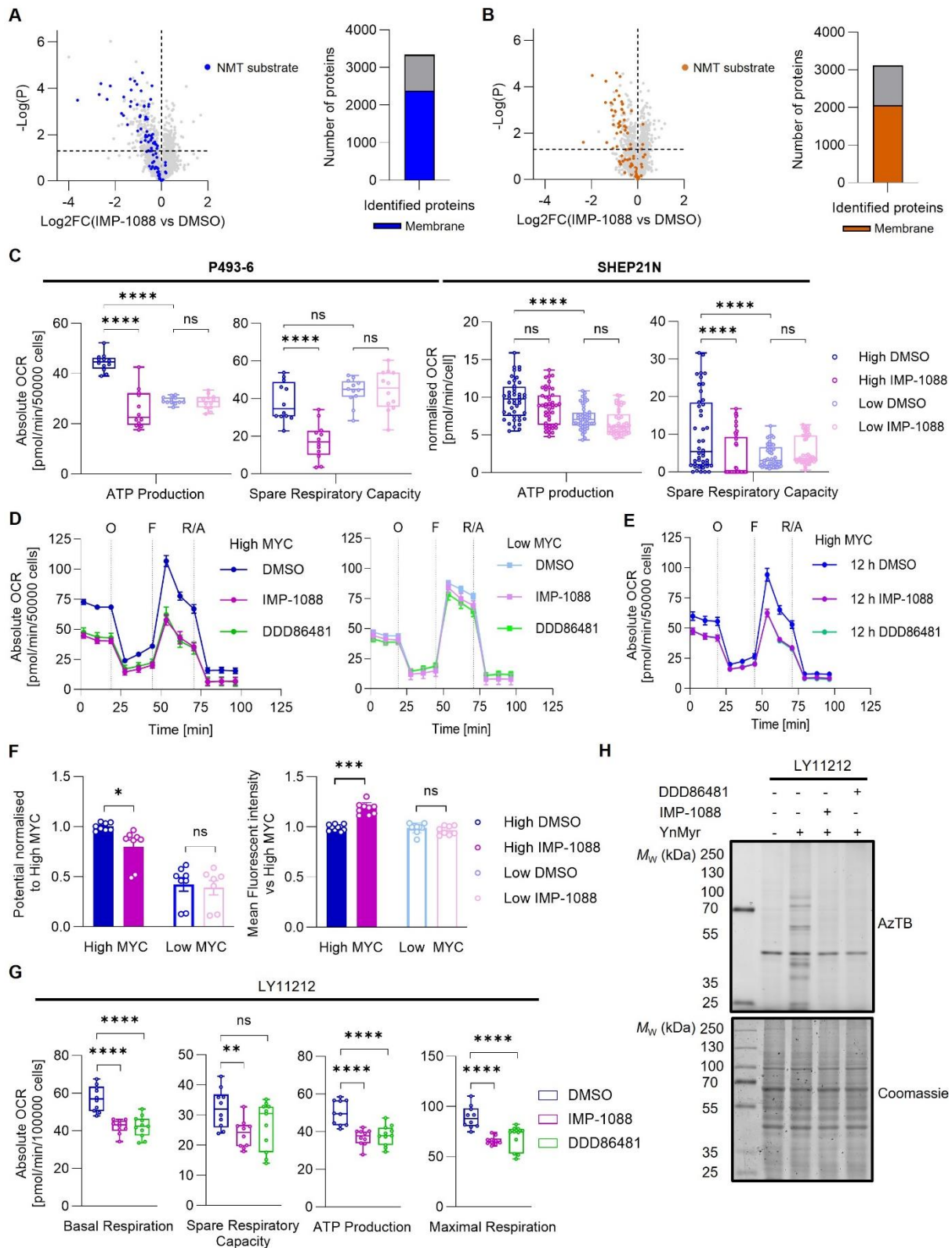


**Figure S3: NMTi induces mitochondrial dysfunction selectively in high MYC contexts, related to Figure 3. (A and B)** Co-translational NMT substrates (left) and membrane-localized proteins (right) identified in detergent fractions from P493-6 **(A)** or SHEP21N **(B)** lysates. **(C)** Parameters of mitochondrial function in P493-6 and SHEP21N cells calculated using data in Fig. 3D. **(D)** OCR of P493-6 cells (high and low MYC) upon treatment with IMP-1088 (100 nM), DDD86481 (1  $\mu$ M) or DMSO control for 18 h. **(E)** OCR of P493-6 cells (high MYC) upon treatment with IMP-1088 (100 nM), DDD86481 (1  $\mu$ M) or DMSO control for 12 h. **(F)** Impact on mitochondrial potential (left) by IMP-1088 (100 nM, 18 h) and superoxide production (right) in P493-6 cells (high and low MYC). **(G)** Parameters of mitochondrial function in LY11212 PD cancer cells treated by IMP-1088 (100 nM), DDD86481 (1  $\mu$ M) or DMSO control for 18 h. **(H)** NMTi target engagement in LY11212 cells as determined by in-gel fluorescence assays. P493-6 cells were treated with IMP-1088 (100 nM) or DDD86481 (1  $\mu$ M) and YnMyr for 18 h and lysates subjected to ligation with AzTB. O: oligomycin, F: FCCP, R/A: rotenone and antimycin A. Data in **(C-G)** are shown as mean  $\pm$  s.e.m. of  $n = 3$  biological replicates ns: not statistically significant, \*  $P < 0.05$ , \*\*  $P < 0.01$ , \*\*\*\*  $P < 0.0001$ . Significance was determined by one-way ANOVA for LY11212 samples and two-way ANOVA otherwise.

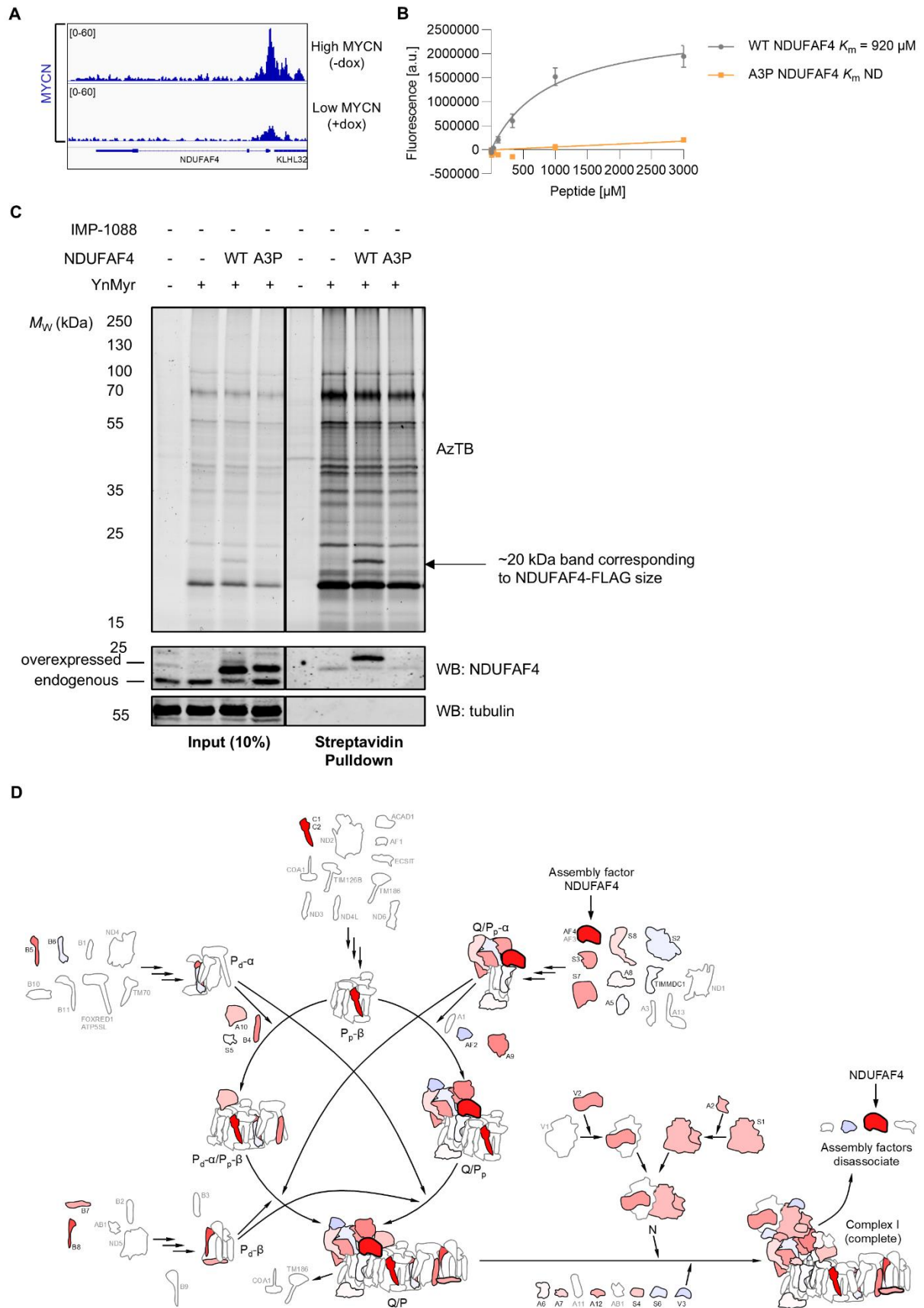


**Figure S4: NDUFAF4 N-myristoylation is associated with complex I assembly, related to Figure 4.** **(A)** MYCN ChIP-Seq tracks for NDUFAF4 in SHEP21N cells. Data were downloaded from GSE80154. **(B)** Calculation of  $K_m$  for NMT activity in synthetic wild-type or A3P NDUFAF4 peptides (aa 2-10) as determined by CPM assay.  $K_m$  was determined using Michaelis Menten kinetics nonlinear regression fit with Prism (GraphPad). Data are shown as mean  $\pm$  s.e.m. of  $n = 3$  independent experiments. ND – not determined. **(C)** Validation of the lack of *N*-myristoylation of the NDUFAF4 A3P mutant as determined by YnMyr pull-down. FLAG-tagged NDUFAF4 was overexpressed in HEK293 cells, which were treated with YnMyr 24 h post-transfection for a further 18 h. Cells were lysed, followed by CuAAC ligation to AzTB and streptavidin pulldown. Note that ligation to AzTB leads to a ca. 1 kDa increase in molecular weight which can be seen in the band shift specifically in labelled and affinity-enriched NDUFAF4. **(D)** Entire assembly scheme for human mitochondrial respiratory complex I as a cartoon representation. Differences calculated in Fig. 4B were color-graded and used as fill for each individual subunit (unidentified subunits in grey). NDUFAF4 is highlighted. Subunit names shortened by omitting 'NDUF'. Figure modified from [S1].



IP PK results							
Time (h)	Plasma levels (ng/ml) of IMP-001320 after IP dosing at 25 mg/kg						
	M4	M5	M6	Mean	±	SD	CV (%)
Body Weight (g)	31	31	31	31	±	0.0	0.00
0.00	0.0	0.0	0.0	0.0	±	0.0	NA
0.08	6750	3550	8270	6190.0	±	2409.3	38.9
0.25	5700	4460	6230	5463.3	±	908.4	16.6
0.50	3730	4090	4310	4043.3	±	292.8	7.2
1.00	2470	2490	2690	2550.0	±	121.7	4.8
2.00	1120	863	1140	1041.0	±	154.5	14.8
4.00	300.0	260.0	315.0	291.7	±	28.4	9.7
8.00	95.3	94.6	90.7	93.5	±	2.5	2.6
24.00	13.4	11.9	13.2	12.8	±	0.8	6.3
IP PK Parameters	M4	M5	M6	Mean	±	SD	CV (%)
Nominal dose (mg/kg)	25.0	25.0	25.0	25.0	±	NA	NA
No. points used for $t_{1/2}$	3	3	3	NA	±	NA	NA
Time points (hr) for $t_{1/2}$	4-24.	4-24.	4-24.	NA	±	NA	NA
R-squared	0.967	0.981	0.957	NA	±	NA	NA
Last time point (hr) for AUC <sub>0-last</sub>	24.0	24.0	24.0	NA	±	NA	NA
C <sub>max</sub> (ng/ml)	6750.00	4460.00	8270.00	6493.3	±	1917.9	29.5
T <sub>max</sub> (hr)	0.08	0.25	0.08	0.14	±	0.1	69.5
AUC <sub>0-last</sub> (ng.hr/ml)	8340.94	7329.62	9019.31	8230.0	±	850.3	10.3
AUC <sub>0-inf</sub> (ng.hr/ml)	8432.69	7410.48	9108.67	8317.3	±	855.0	10.3
AUC <sub>0-inf</sub> /AUC <sub>0-last</sub> (%)	101.10	101.10	100.99	101.1	±	0.1	0.1
Cl <sub>F_obs</sub> (mL/min/kg)	49.41	56.23	45.74	50.5	±	5.3	10.5
T <sub>1/2elim</sub> (hr)	4.75	4.71	4.69	4.7	±	0.0	0.6
MRT <sub>last</sub> (hr)	2.48	2.59	2.32	2.5	±	0.1	5.6
MRT <sub>INF_obs</sub> (hr)	2.79	2.90	2.59	2.8	±	0.2	5.5

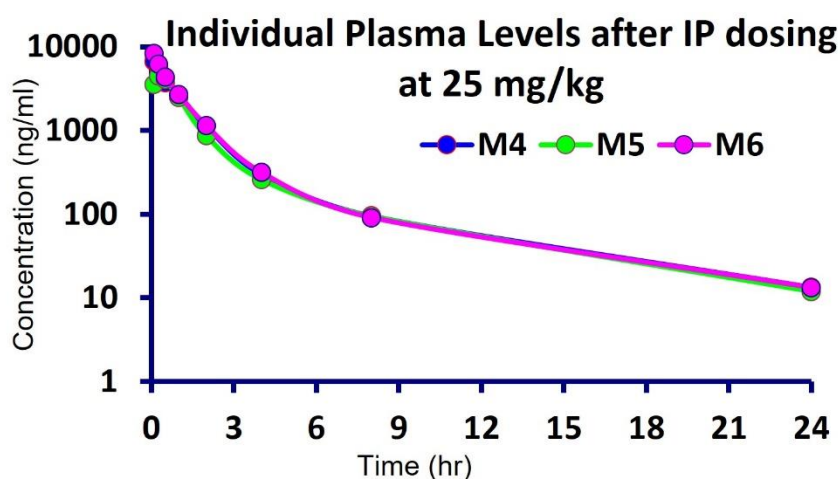


**Figure S5: Pharmacokinetic profile of IMP-1320, related to Figure 5.** IMP-1320 was dosed once at 25 mg/kg interperitoneally (IP, n = 3, mice M4-M6), and plasma levels measured by high performance liquid chromatography-mass spectrometry (HPLC-MS) at the time points indicated. N/A – not applicable.

IP PK results							
Time (h)	Plasma levels (ng/ml) DDD86481 after IP dosing at 25 mg/kg						
	M7	M8	M9	Mean	±	SD	CV (%)
Body Weight (g)	31	32	32	32	±	0.58	1.82
0.00	0.0	0.0	0.0	0.0	±	0.0	NA
0.08	23800.0	28900.0	36100.0	29600.0	±	6179.8	20.9
0.25	56800.0	69200.0	61400.0	62466.7	±	6268.4	10.0
0.50	59000.0	62400.0	54200.0	58533.3	±	4119.9	7.0
1.00	53500.0	66600.0	51800.0	57300.0	±	8098.8	14.1
2.00	40000.0	47800.0	37200.0	41666.7	±	5493.0	13.2
4.00	39300.0	55100.0	42300.0	45566.7	±	8391.3	18.4
8.00	13000.0	20400.0	13000.0	15466.7	±	4272.4	27.6
24.00	24.6	18.8	14.0	19.1	±	5.3	27.7

IP PK Parameters	M7	M8	M9	Mean	±	SD	CV (%)
Nominal dose (mg/kg)	25.0	25.0	25.0	25.0	±	NA	NA
No. points used for $t_{1/2}$	3	3	3	NA	±	NA	NA
Time points (hr) for $t_{1/2}$	4-24	4-24	4-24	NA	±	NA	NA
R-squared	0.997	0.994	0.997	NA	±	NA	NA
Last time point (hr) for AUC <sub>0-last</sub>	24.0	24.0	24.0	NA	±	NA	NA
C <sub>max</sub> (ng/ml)	59000.0	69200.0	61400.0	63200.0	±	5332.9	8.4
T <sub>max</sub> (hr)	0.5	0.25	0.25	0.3	±	0.1	43.3
AUC <sub>0-last</sub> (ng.hr/ml)	304221.8	404005.4	303904.6	337377.3	±	57701.8	17.1
AUC <sub>0-inf</sub> (ng.hr/ml)	304287.3	404051.2	303938.9	337425.8	±	57699.5	17.1
AUC <sub>0-inf</sub> /AUC <sub>0-last</sub> (%)	100.02	100.01	100.01	100.0	±	0.0	0.01
Cl <sub>F_obs</sub> (mL/min/kg)	1.37	1.03	1.37	1.3	±	0.2	15.6
T <sub>1/2elim</sub> (hr)	1.85	1.69	1.70	1.7	±	0.1	5.0
MRT <sub>last</sub> (hr)	4.01	4.22	3.97	4.1	±	0.1	3.3
MRTINF_obs (hr)	4.01	4.22	3.97	4.1	±	0.1	3.3
%BA*	158.33	210.24	158.15	175.6	±	30.0	17.1

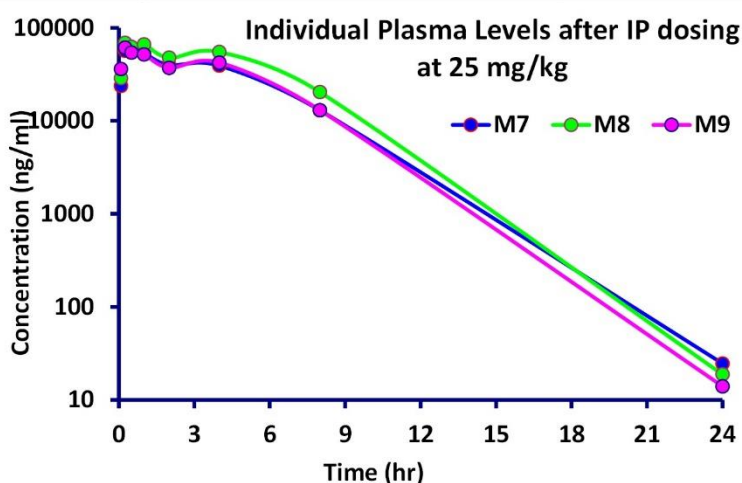


**Figure S6: Pharmacokinetic profile of DDD86481, related to Figure 5.** DDD86481 was dosed once at 25 mg/kg interperitoneally (IP, n = 3, mice M7-M9), and plasma levels measured by high performance liquid chromatography-mass spectrometry (HPLC-MS) at the time points indicated. The concentration of DDD86481 remains above 1  $\mu$ M (a concentration sufficient to fully suppress NMT activity in cells in culture) for ca. 16 hours post dosing, dropping to ca. 30 nM at 24 hours. N/A – not applicable.

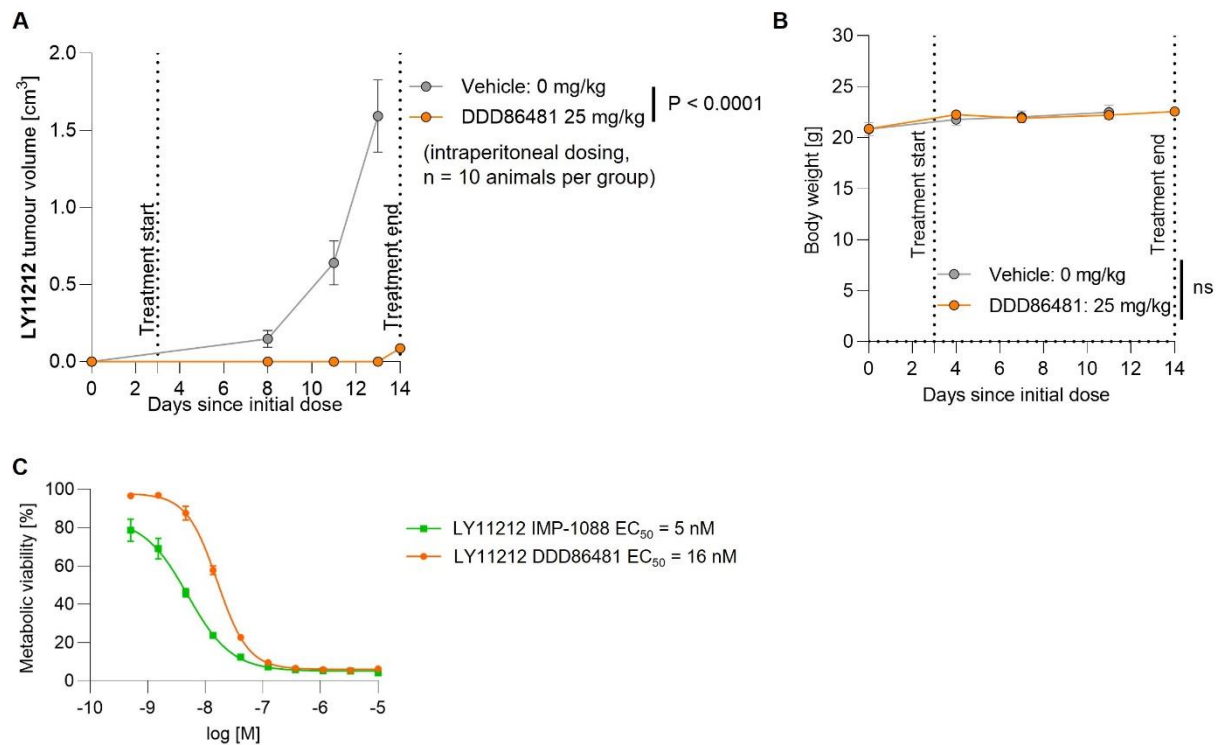


**Figure S7: NMTi reduces tumor burden in LY11212 PD xenograft models, related to Figure 5.** (A) Impact of intraperitoneally administered DDD86481 (25 mg/kg QD) on the growth of PDX in vivo using PD cancer cells LY11212 that carry a MYC translocated allele (n = 10 mice per group; error bars represent mean  $\pm$  s.e.m.; time-adjusted ANOVA). (B) Change in mouse body weight between the start and end point of the experiments for the LY11212 PDX, comparing treated and control (t-test, paired). (C) Metabolic viability was measured using the CellTiter-Blue assay on LY11212 PD cancer cells treated with a range of concentrations of IMP-1088 and DDD86481 for 72 h in vitro. Data are shown as mean  $\pm$  s.e.m. of n = 3 biological replicates.

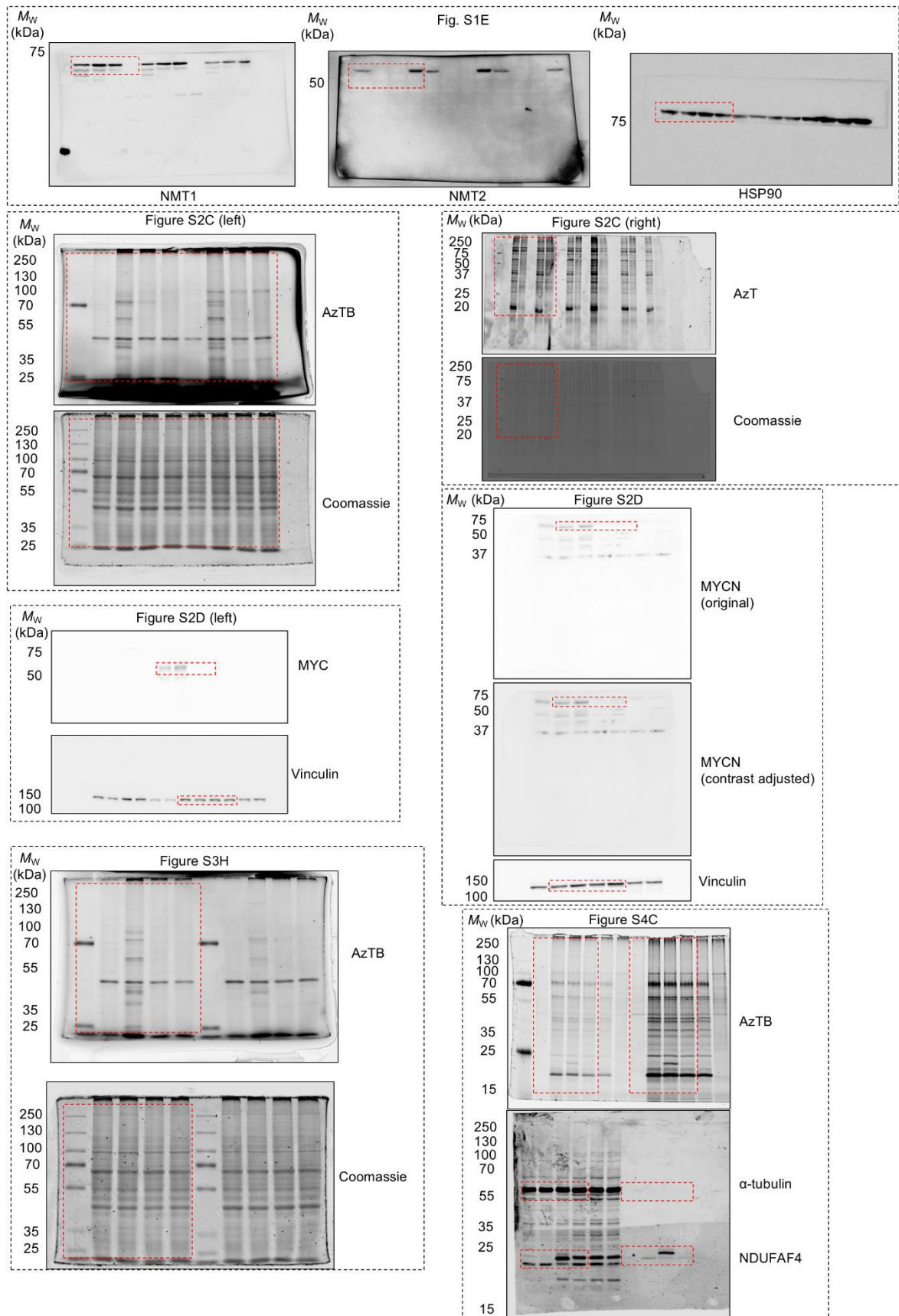


**Figure S8: Original image data for blots and gels, related to Figures 2 and 4.**



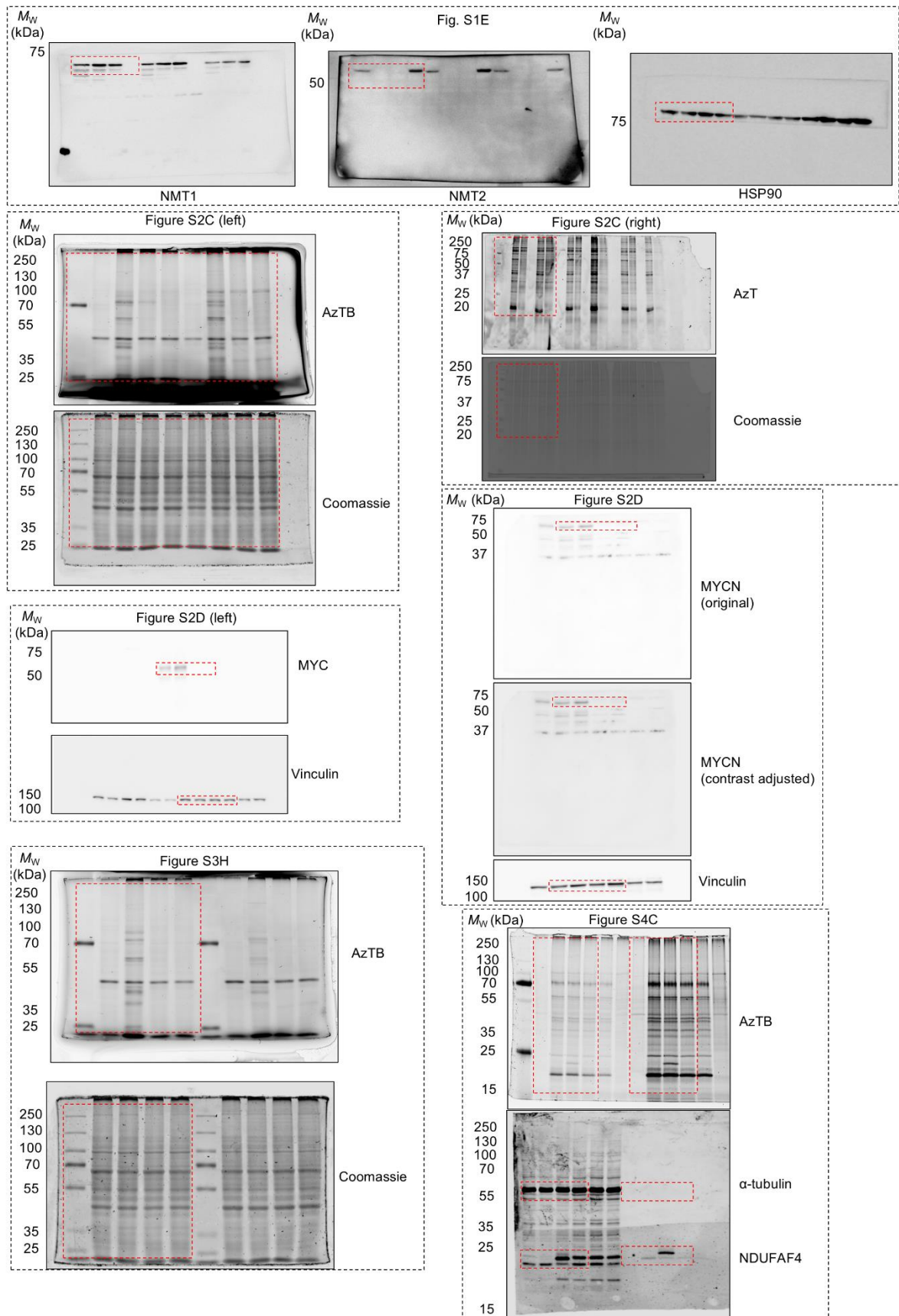
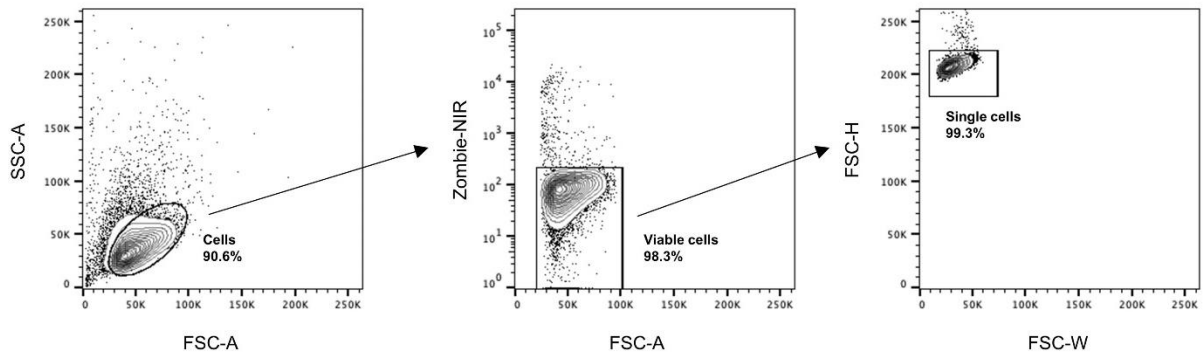
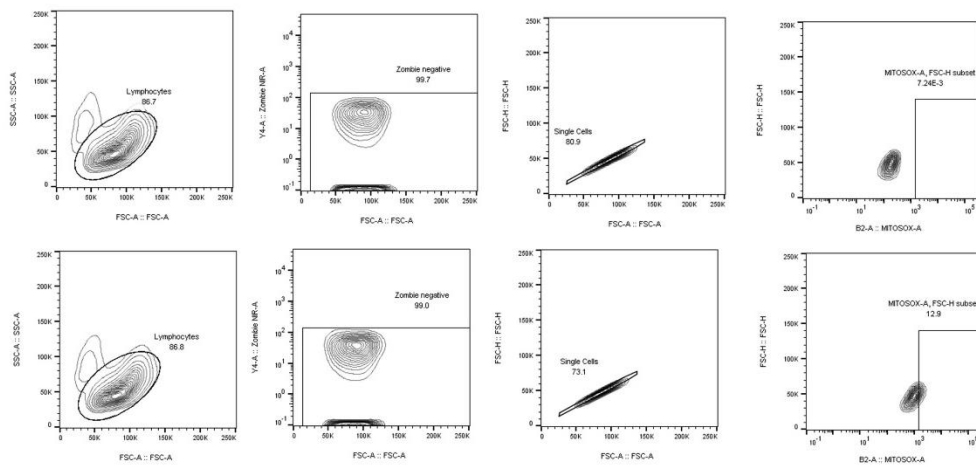


**Figure S9: Original image data for blots and gels, related to Figures S1-4.**

### General gating strategy



### Mitosox experiment gating strategy control/treated (Top and Bottom)



### MitoTracker experiment gating strategy comparing control/treated (Top and Bottom)

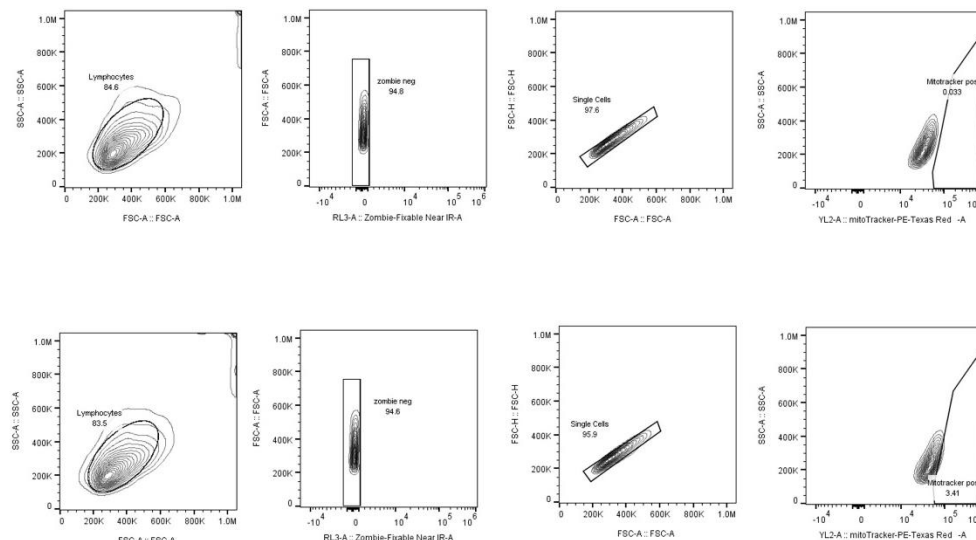


**Figure S10: Examples of gating strategies for flow cytometry experiments, related to STAR Methods.**

gRNA/Primer	Sequence
NMT1 gRNA 1F	TTTCTTGGCTTTATATATCTTGTGGAAAGGACGAAACACC <b>ggcgaagtgggtaacaccca</b>
NMT1 gRNA 1R	GACTAGCCTTATTTTAACTTGCTATTTCTAGCTCTAAAAC <b>tggggtgttcaccacttcgcc</b>
NMT2 gRNA 1F	TTTCTTGGCTTTATATATCTTGTGGAAAGGACGAAACACC <b>ggctgtgtacaccgcgggag</b>
NMT2 gRNA 1R	GACTAGCCTTATTTTAACTTGCTATTTCTAGCTCTAAAAC <b>ctccccgcgggtgtacacagcc</b>
NMT2 gRNA 2F	TTTCTTGGCTTTATATATCTTGTGGAAAGGACGAAACACC <b>gaaaaactcaagtttgat</b>
NMT 1F Sequencing	TCTTTGCCAGCAGAGAGGAT
NMT 1R Sequencing	CTGGCGGATATTGTCCTTGT
NMT2 1F Sequencing	ATAAGTGCCATCCCAGCAAA
NMT2 1R Sequencing	TGATCGATGCCAGTATCTGC
NMT2 2F Sequencing	GATGTATTCAATGCACTGGATT
NMT2 2R Sequencing	CACTTACCTTTTCAGAATCTGT
NDUFAF4 F WT	CTAGACTCGAGGGTACCGGATCCATGGGAGCACTAGTGATTGCGG
NDUFAF4 F G2A	CTAGACTCGAGGGTACCGGATCCATGGccGCACTAGTGATTGCGGGTATC
NDUFAF4 F A3P	CTAGACTCGAGGGTACCGGATCCATGGGAcCcCTAGTGATTGCGGGTATC
NDUFAF4 R	CTTGTCATCGTCGTCCTTGTAGTCTTTTGATCGTATTGCTTTCTTGTCTTCA GG
NDUFAF4 geneblock	atgggagcactagtgattcgcggtatcaggaattcaacctagagaaccgagcggaaacgggaaatcagcaa gatgaagccctctgctgctcccagacacccctctaccaacagcctcctgcgagagcagattagctctatccag aagttaaggagagattgctcgtaaaagatgaaaagctgctgctgttctaaaagatgtgtatgttgattccaaag atcctgtgtcttcctgcaggtaaaagctgctgaaacatgtcaagagccgaaggaattcagattgccgaaagac catcatTTTgatatgataaatattaagagcattcccaaaggcaaaattccattgtagaagcattgacacttctcaa taatcataaActtttccagaaacctggactgctgagaaaataatgcaggaataaccagttagaacagaaagat gtgaattcttcttaaatatttgttactttgaagtgcgaatctccctcctgaagacaagaaagcaatacgaatcaa aa

**Table S2. gRNA, cloning and sequencing primers, related to STAR Methods.**

## **SUPPLEMENTAL REFERENCES**

- [S1]. Guerrero-Castillo, S., Baertling, F., Kownatzki, D., Wessels, H.J., Arnold, S., Brandt, U., and Nijtmans, L. (2017). The Assembly Pathway of Mitochondrial Respiratory Chain Complex I. *Cell Metab.* 25, 128-139. 10.1016/j.cmet.2016.09.002.